Load-Slip Response of Larger Diameter GFRP Truss-Action Shear Connectors for Precast Concrete Insulated Wall Panels

Sergio Arevalo and Douglas Tomlinson

1 Introduction

Precast concrete insulated wall panels have been used as exterior walls for over fifty years. These systems are advantageous because they combine structural and thermal resistance into a single unit that allows for efficient and quick-to-install walls. A typical insulated wall panel is comprised of a layer of foam insulation surrounded by two concrete layers (known as wythes). Shear connectors connect the two concrete wythes together. Traditionally, steel connectors were used but as energy codes evolve (e.g. the building energy codes requiring designers to account for thermal bridging through the insulation (NRCan 2016), materials with lower thermal conductivity (such as GFRP) have become more popular as shear connectors.

The structural response of insulated panels is heavily influenced by connector material and arrangement (PCI 2011). Traditional design approaches have focused on connector strength, but wall response is more significantly affected by connector stiffness. Walls with stiff connectors are advantageous because they transfer forces more efficiently which allows designers to specify thinner (i.e. lighter) walls. However, stiff connectors may also lead to thermal bowing concerns which can be significant in longer panels (PCI 2011). The performance (i.e. strength, stiffness, and ductility) of connector systems is usually assessed using direct shear push-through tests constructed using the same connectors, reinforcement, and wythe arrangement as a full-sized panel. Researchers have used push-through tests to evaluate pin-type GFRP and steel connectors (Woltman et al. 2013), common commercially available

S. Arevalo · D. Tomlinson (✉)

Department of Civil and Environmental Engineering, University of Alberta, 9211 116 St NW, Edmonton, AB, Canada
e-mail: dtomlins@ualberta.ca

S. Arevalo
e-mail: sarevalo@ualberta.ca

connectors (Naito et al. 2012), FRP mesh systems (Bunn 2011; Kim and You 2015), and Basalt FRP inclined connectors (Tomlinson et al. 2016). Outcomes of these tests have been used to evaluate connector systems and develop numerical models that predict the strength and stiffness of FRP shear connectors. Though many connectors have been evaluated to date, there is limited data on panels constructed with larger diameter inclined shear connectors (i.e. greater than 10 mm diameter). Previous work on inclined connectors (Tomlinson et al. 2016) indicated that larger connectors may be more efficient than smaller connectors since they are better able to resist compression loads. This paper looks to expand the literature to include larger connectors and call attention to new failure modes that may occur with larger connectors.

2   Experimental Program

A connector arrangement consisting of large (>10 mm diameter) GFRP bars arranged in an 'X' shape is proposed. Advantages of larger connectors include greater stiffness leading to more rigid panels and easier construction (i.e. fewer connectors need to be inserted). An illustration of connectors placed at 600 mm along a 6 m long panel is shown in Fig. 1. The wythes and rigid insulation in the panel are 75 mm thick, typical of current construction. The connectors are comprised of two 250 mm long GFRP bars inserted at 45° to the panel face and embedded 71 mm into each wythe. GFRP was used since it has lower thermal conductivity (i.e. more thermally efficient) than steel connectors. GFRP connectors have been successfully used in previously tested panels (Naito et al. 2012; Kim and You 2015). The "X" orientation ensures that connectors are providing truss action in both tension and compression. To assess connector performance, a subset of the full panels was tested under double shear. Each specimen is 600 × 375 × 300 mm in size. The 600 mm length represents the expected centre-to-centre spacing of connectors for full-scale panels. Specimens were designed to represent two back-to-back panels to create load symmetry, an approach commonly used to simplify the test setup.
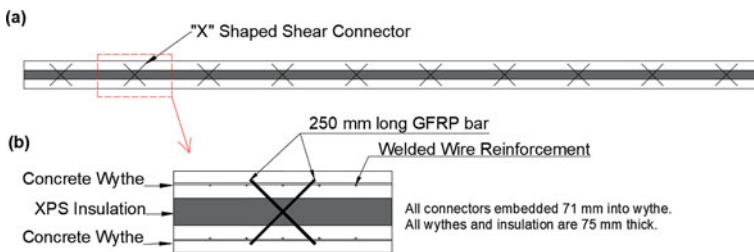

Fig. 1 Illustration of connector design in **a** full-sized panel (6 m long panel with connectors spaced at 600 mm) and **b** segment of full panel showing connector

Table 1 Test matrix (Arevalo 2019)

Test identifier	Nominal GFRP bar diameter, mm	Nominal bar area (per bar), mm²	Insulation bond
3B	9.52	71.2	Bonded
3U	9.52	71.2	Unbonded
4B	12.7	127	Bonded
4U	12.7	127	Unbonded
5B	15.9	199	Bonded
5U	15.9	199	Unbonded

The test matrix, originally presented as part of the primary author's thesis with additional insight added in this paper, is shown in Table 1. Three bar sizes (nominal diameters of 9.53, 12.7, and 16.0 mm) were tested to investigate size influence on strength, stiffness, and failure mode. For each bar size, two types of specimens were tested. One type (bonded) left the bond between the insulation and concrete intact while the other type (unbonded) broke the insulation-concrete bond using a thin plastic sheet. The insulation bond was shown to be significant in previous research (Woltman et al. 2013; Tomlinson et al. 2016). Tests are identified with a 2-digit code with the first digit representing bar diameter: 3 = 9.53 mm, 4 = 12.7 mm, and 5 = 16.0 mm while the second digit identifies bond quality: B = bonded and U = unbonded. In total, six specimen types were tested and three specimens were tested from each type (i.e. 18 tests total).

2.1 Materials

Specimens were constructed with self-consolidating concrete. The 28-day concrete strength was 52 MPa and the elastic modulus, measured using a compressometer, was 23.5 GPa. Commercially available GFRP rebar was used as the connectors. The GFRP's average tensile strength and elastic modulus, determined from tensile tests, were 1420 MPa and 60.5 GPa. There were no noticeable differences in strength and modulus across the tested diameters. Wythes were reinforced with steel welded wire mesh (5.8 mm diameter, 100 mm spacing in both directions). Extruded polystyrene (XPS) foam was used as insulation.

2.2 Test Setup and Instrumentation

The test setup is shown in Fig. 2. The outer wythes of the specimen were placed on 75 × 75 mm steel supports. Two steel side supports were clamped on either side of the specimen to prevent wythe rotation. Specimens were loaded at 1 mm/min using
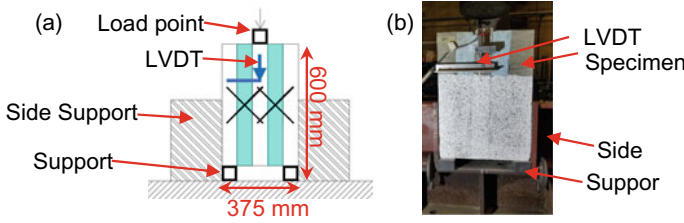
Fig. 2 Test setup **a** schematic and **b** photograph

a 360 kN actuator. Two 25 mm Linear Variable Differential Transformers (LVDT) were mounted on the front and back of the specimen to measure relative wythe slip.

3   Results and Discussion

Load-slip results are shown in Fig. 3. These results are the averaged response of the three tests from each specimen type. Load-slip responses were similar across all parameters. There was an initial high-stiffness region that lasted until the proportional limit (caused by insulation bond failure and/or the onset of non-linear FRP response caused by fibres slipping against each other from dowel action). After the proportional limit, stiffness decreased but load continued to increase until the peak load was reached. Once the peak load was reached, the load steadily decreased as one bar failed and redistributed loads to other bars.

Table 2 presents a summary of the test results. In Table 2, the stiffness was found with Eq. 1.

$$k = \frac{F_{0.4U} - F_{0.1U}}{\Delta_{0.1U} - \Delta_{0.1U}} \tag{1}$$

A secant is taken between 10% ($F_{0.1U}$) and 40% ($F_{0.4U}$) of the peak load using a similar process to finding the stiffness of a concrete cylinder. The corresponding
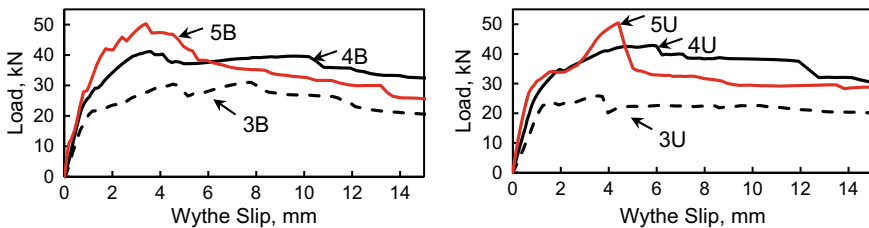

Fig. 3 Load-slip response for **a** bonded and **b** unbonded specimens. The load carried by one connector pair (i.e. half load cell reading) is reported. Curves are averages of three tests

Table 2 Test results. Load and stiffness values are based on the total applied load. First number is the average of the three tests for each specimen type, ± results are standard deviations

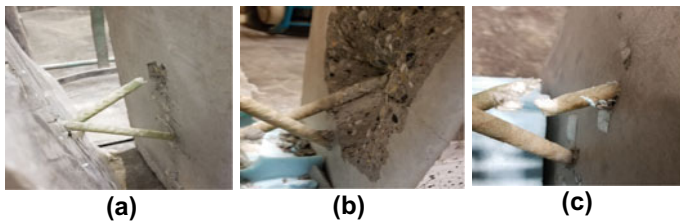| Test identifier	Proportional limit, kN	Peak load, kN	Displacement at peak load, mm	Stiffness, kN/mm (Eq. 1)
3B	39.7 ± 7.9	69.2 ± 4.4	5.66 ± 1.91	63.0 ± 3.8
3U	35.5 ± 12.7	52.1 ± 3.7	3.02 ± 1.39	51.8 ± 6.4
4B	39.1 ± 2.9	83.2 ± 9.6	4.82 ± 0.47	81.8 ± 10.8
4U	34.0 ± 3.8	88.2 ± 11.1	5.01 ± 2.85	78.4 ± 10.6
5B	43.6 ± 2.3	95.3 ± 11.6	6.33 ± 2.70	114 ± 11.0
5U	25.8 ± 3.3	100 ± 12.3	2.56 ± 1.57	118 ± 12.0

(a)   (b)   (c)

Fig. 4 Failure modes **a** tension pull-out, **b** concrete crushing, and **c** compression connector crush

slip at these two points are $\Delta_{0.1U}$ $\Delta_{0.4U}$. If the proportional limit is less than $F_{0.4U}$, then a secant between $F_{0.1U}$ and the proportional limit was used.

3.1 Effect of Parameters on Failure Mode

Each specimen was dissected to evaluate failure modes. Tests 3B and 3U failed by compression connector failure and/or tension connector pull-out. Tests 4B and 4U failed by tension connector pull-out and/or concrete crushing around the compression connector. Tests 5B and 5U all had concrete crushing failure around the compression connector with evidence that connectors punched through the far side of the panel. Examples of these failures are shown in Fig. 4. Multiple failure modes were evident in some specimens since they were loaded to slips of 15 mm, causing potentially multiple connectors to fail by different means.

3.2 Effect of Parameters on Strength and Stiffness

The relationship between peak load, estimated connector stress, and stiffness relative to the bar area is given in Fig. 5a The peak load average increased by 20% from 3
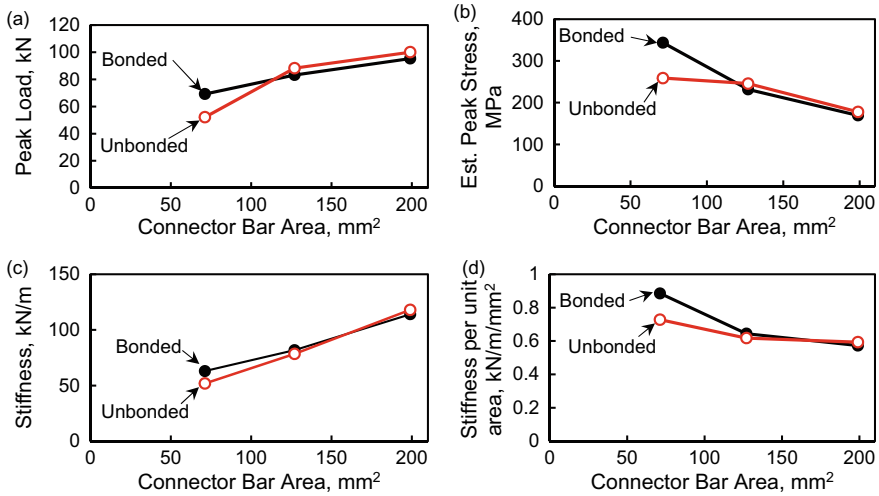
Fig. 5 Parameter effect on **a** peak load, **b** peak stress, **c** stiffness, and **d** stiffness per unit area

to 4B, and by 15% from 4 to 5B. For unbonded specimens, this increase was 69% from 3 to 4U and 14% from 4 to 5U. This relation shows a non-linear increase in peak load as shear connector diameter increases. To relate this to the area, the peak axial stress carried by the shear connectors, σ_{SC}, was estimated using Eq. 2.

$$\sigma_{SC} = \frac{P_U}{n A_{sc} \sin\theta} \tag{2}$$

where P_U is the peak load, θ is the insertion angle (45°). A_{sc} is the connector area, and n is the number of bars (4 in all tests). Equation 2 assumes small deformations and that the force is transferred entirely by truss action. Previous work (Tomlinson et al. 2016), indicates that this assumption, though not representing the actual connector stress, is valid (<5% error) for truss-type connectors similar to the ones tested here. Peak stress decreased as connector size increased. For bonded tests, the peak stress decreased 26% from 3 to 4B, and 37% from 4 to 5B. For unbonded tests, the decrease was 4.8% from 3 to 4U and 27% from 4 to 5U. Based on this, it is more efficient to use more, smaller connectors (such as 9.5 mm) than fewer larger connectors since smaller connectors carry higher stresses before failure. Since Tomlinson et al. (2016), noticed the opposite with small connectors, this indicates that 9.5 mm connectors may be the most efficient (best compression and tension resistance) for this type of connection system. However, Fig. 5b shows limited gains from 12.7 to 16.0 mm, indicating that the 12.7 mm bar is most efficient for strength.

Stiffness increased as connector size increased (Fig. 5c). Stiffness increased 30% from 3 to 4B and 39% from 4 to 5B. For unbonded specimens, stiffness increased 51% from 3 to 4U and 50% from 4 to 5U. The decrease from bonded to unbonded

specimens was 22% for 3B and 3U but there was effectively no change between bonded and unbonded specimens for the larger diameters. Though stiffness increased with connector size, there is a diminishing return since the stiffness per unit area of the bars decreases significantly once bars larger than 9.5 mm are used (Fig. 5d).

For both strength and stiffness, the insulation bond contribution reduces as connector size increases. This indicates that the large, truss-type connectors dominate behaviour and insulation contribution is negligible, which was not the case in some tests with smaller connectors (Tomlinson et al. 2016).

3.3 Comparison to Other Connectors

The test results are compared to those from other researchers in Table 3.

Though other tests had different parameters (e.g. connector materials, insulation thickness, concrete strength), general trends can be observed. Connectors used in this study have much higher shear flow than dowel-type 9.53 and 12.7 mm GFRP connectors (Woltman et al. 2013) and even higher capacity than 37 × 9.5 mm dowel connectors (Naito et al. 2012) illustrating truss action effectiveness. These tests were also considerably stronger than those by Tomlinson et al. (2016) which illustrates the effect of increasing bar diameter. The FRP grids tested by Kim and You (2015) and Bunn (2011) have a similar shear flow to the 9.5 and 12.7 mm bars. Similar trends were observed between for shear connection stiffness. This illustrates that 9.5 and 12.7 mm 'X' shape shear connectors have similar shear flow and stiffness as

Table 3 Shear flow and stiffness values reported in literature

Study	Connector type	Connector size	Connector arrangement	Peak shear flow, kN/m	Normalized stiffness, kN/mm/m
Current	GFRP bar	9.5–16 mm	±45°	40.0–93.2	53–98
Tomlinson et al. (2016)	Basalt FRP bar	4–8 mm	90°, ±45°	5.7–31	N/A
Woltman et al. (2013)	GFRP bar	6.3–12.7 mm	90°	4.0–14.0	N/A
Naito et al. (2012)	GFRP composite pin (400 mm spacing)	37 × 9.5 mm	90°	30.2	18
Kim and You (2015)	GFRP grid	60 mm²/m	±45°	58–76	N/A
Bunn (2011)	Carbon FRP grid	40 mm²/m	±45°	72.5	65

N/A—results not reported

distributed FRP grids but that the stiffness can be increased further with the 16.0 mm connectors.

4 Conclusion

This paper discussed the push-through experimental program to investigate larger diameter GFRP truss-type connectors. Shear connectors with 9.53, 12.7, and 16.0 mm diameters were investigated to evaluate their stiffness, strength, and failure modes. The following was observed:

1. Peak load increased with connector size; connector failure stress decreased as connector size increased. The lower diameter connectors (9.5, 12.7 mm) are more efficient (i.e. reach higher stress) compared to the 16.0 mm connectors. The larger connectors fail by concrete crushing and blow-out which prevents them from reaching higher capacities.
2. Connector stiffness increased with connector diameter. Similar to what was seen with strength, there were diminishing returns with respect to connector efficiency as diameter increased.
3. The insulation bond had a significant effect on the tests with 9.5 mm connectors but this effect was negligible in tests that used 12.7 and 16.0 mm connectors.
4. Large, truss-type GFRP bars can achieve strengths and stiffnesses that exceed tests with FRP grids. However, caution must be exercised in design to ensure that connectors can be designed considering concrete crushing and blow-out of wythe concrete.

Though the goal of this program was to develop a stiff connector, there are situations where low stiffness connectors are needed (e.g. if thermal bowing is a large concern). The authors recommend expanding this study to investigate smaller and larger connectors to confirm if the diminishing effect of stiffness for these connectors is observed over a wider range. They also recommend testing other insulation types to see if the insulation contribution is still lost for larger diameter bars with other insulation types.

References

Arevalo S (2019) Experimental investigation of thermal bowing for concrete insulated wall panels. MSc thesis, University of Alberta, Edmonton

Bunn W (2011) CFRP grid/rigid foam shear transfer mechanism for precast prestressed concrete sandwich wall panels. MSc thesis, North Carolina State University, Raleigh

Kim JH, You Y-C (2015) Composite behavior of a novel insulated concrete sandwich wall panel reinforced with GFRP shear grids: effects of insulation types. Materials 8:899–913

Naito C, Hoemann J, Beacraft M, Bewick B (2012) Performance and characterization of shear ties for use in insulated precast concrete sandwich wall panels. J Struct Eng 138(1):52–61

National Resources Canada (2016) Energy fact book 2016–2017. Office of Energy Efficiency. Ottawa, Ontario

Precast Concrete Institute (2011) State of the art of precast/prestressed concrete sandwich wall panels. PCI J 56(2):131–176

Tomlinson D, Teixeira N, Fam A (2016) New shear connector design for insulated concrete sandwich panels using basalt fiber-reinforced polymer bars. J Compos Constr 20(4):1–13

Woltman G, Tomlinson D, Fam A (2013) Investigation of various GFRP shear connectors for insulated precast concrete sandwich wall panels. J Compos Constr 17(5):711–721